

When Unsupervised Domain Adaptation meets One-class Anomaly Detection: Addressing the Two-fold Unsupervised Curse by Leveraging Anomaly Scarcity

Nesryne Mejri¹, Enjie Ghorbel^{2,1}, Anis Kacem¹, Pavel Chernakov¹,
Niki Foteinopoulou¹, Djamilia Aouada¹

¹Interdisciplinary Centre for Security, Reliability and Trust (SnT), University of Luxembourg

²Cristal Laboratory, National School of Computer Sciences, University of Manouba

{nesryne.mejri, anis.kacem, pavel.chernakov, niki.foteinopoulou, djamilia.aouada}@uni.lu
enjie.ghorbel@isamm.uma.tn

Abstract

This paper introduces the first fully unsupervised domain adaptation (UDA) framework for unsupervised anomaly detection (UAD). The performance of UAD techniques degrades significantly in the presence of a domain shift, difficult to avoid in a real-world setting. While UDA has contributed to solving this issue in binary and multi-class classification, such a strategy is ill-posed in UAD. This might be explained by the unsupervised nature of the two tasks, namely, domain adaptation and anomaly detection. Herein, we first formulate this problem that we call **the two-fold unsupervised curse**. Then, we propose a pioneering solution to this curse, considered intractable so far, by assuming that anomalies are rare. Specifically, we leverage clustering techniques to identify a dominant cluster in the target feature space. Posed as the normal cluster, the latter is aligned with the source normal features. Concretely, given a one-class source set and an unlabeled target set composed mostly of normal data and some anomalies, we fit the source features within a hypersphere while jointly aligning them with the features of the dominant cluster from the target set. The paper provides extensive experiments and analysis on common adaptation benchmarks for anomaly detection, demonstrating the relevance of both the newly introduced paradigm and the proposed approach. The code will be made publicly available.

1. Introduction

Anomaly Detection (AD) can be seen as the identification of outliers deviating from a usual pattern. The growing interest for AD in both academia and industry is mainly due to its relevance in numerous practical scenarios, such as early disease detection in medical imaging [1, 17] and industrial inspection [3, 8, 24, 25, 39]. By definition, anomalies rarely

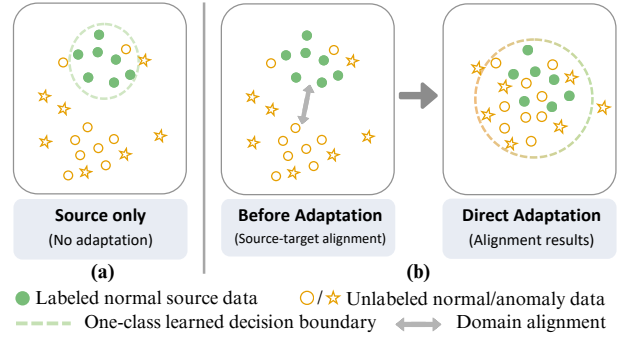


Figure 1. **Illustration of the two-fold unsupervised curse:** (a) The decision boundary learned from the source set without any adaptation does not allow generalization to the target domain. (b) Direct alignment of the unlabeled target with the one-class source features leads to the confusion of normal and abnormal samples.

occur. Annotating anomalous data is, therefore, often difficult and costly [4, 16, 39], hindering the collection of large-scale datasets. As a result, state-of-the-art methods mostly tackle AD as an unsupervised problem [13, 34], where the objective is to learn from the normal class.

Despite achieving promising results, recent approaches in AD [8, 16, 33, 38, 40] typically assume that training and inference data are drawn from the same distribution. This assumption does not always hold in unconstrained scenarios, where a *domain shift* [29] between training and testing data can naturally arise due to varying setups, such as different lighting conditions and variations in object pose [4]. As a result, a model trained on a dataset sampled from a given domain, usually called *source* dataset, will show degraded performance when tested on a dataset from a different domain, generally termed *target* dataset. For instance, an AD model for medical imaging trained on images acquired using a given Medical Resonance Imaging (MRI) device can fail to generalize to samples captured with a different MRI system.

To reduce such a domain gap while avoiding costly annotation efforts, Unsupervised Domain Adaptation (UDA) [18, 42] has proven to be an effective solution in binary and multi-class classification tasks [18, 36]. UDA aims at learning domain-invariant features by relying on labeled source and unlabeled target data at the same time. However, the task of **unsupervised** domain adaptation for **unsupervised** anomaly detection (UAD) is ill-posed as the goal is to: *align the source and the target feature distributions using only normal source data and unlabeled target data formed by both normal and anomalous samples* (see Figure 2 (c)). Hence, a direct extension of standard UDA techniques developed for binary/multi-class classification [18, 42] would not be applicable, as these methods usually aim at minimizing the distance between the estimated distributions from the entire source and target training sets. Indeed, this would lead to the erroneous alignment of both normal and anomalous target samples with normal source samples, as illustrated in Figure 1 (b). Given the learned decision boundary, this would lead to the confusion of normal and abnormal samples from the target set. As it requires addressing two unsupervised tasks simultaneously, we refer to this described problem as the *two-fold unsupervised curse*.

To the best of our knowledge, no prior work has tried to address this two-fold unsupervised challenge, *i.e.*, UDA for one-class image anomaly detection described in Figure 2 (c). Indeed, related works have mainly simplified the problem by either (1) assuming the availability of labeled abnormal and normal source data, resulting in UDA for a binary classification setting [19] (see Figure 2 (a)), or (2) maintaining the source one-class setup while accessing only few normal target data referred to as few-shot supervised adaptation for unsupervised anomaly detection [7, 19, 22, 23, 43] (see Figure 2 (b)). Nevertheless, annotating a few samples might still be constraining, particularly in the field of anomaly detection, where expert knowledge is often needed, such as for tumor annotation in medical images [1, 17] or for industrial inspection [8, 24, 40]. Moreover, few-shot approaches are known to be prone to overfitting issues since few shots cannot fully represent the normal target distribution [37]. This calls for a fully unsupervised domain adaptation approach that leverages the diversity of the available large unlabeled target datasets.

In this paper, we propose solving the two-fold unsupervised curse by leveraging the fact that the occurrence of anomalies tends to be rare. We herein propose the first unsupervised domain adaptation framework for unsupervised image anomaly detection. Our solution starts by identifying a dominant cluster assumed to be formed by normal target data and then aligning it with normal source samples. Specifically, our method utilizes a trainable ResNet-based [15] feature extractor to process both the source and target features. A frozen CLIP visual en-

coder [30] is also used to generate corresponding target features, which are then clustered using K-means to identify the samples of the dominant cluster. These samples are mapped into the ResNet-based [15] feature space and aligned with the source features. For the domain adaptation task, a contrastive strategy [26, 30] ensures the similarity between the dominant target cluster and normal source samples, while for the anomaly detection task, a Deep Support Vector Data Description (DSVDD) [33] objective enforces feature compactness on the normal source data. Our framework is modular, allowing for flexible component changes, and supports various adaptation strategies, including statistical and adversarial alignment. Experiments performed on standard UDA benchmarks [28, 35, 41] for semantic anomaly detection [38] demonstrate its effectiveness. Our approach achieves state-of-the-art (SoA) performance, even compared to few-shot methods.

Contributions. The main contributions of this work can be summarized as follows:

- The two-fold unsupervised curse of UDA for one-class anomaly detection is formalized, and the induced challenges are outlined.
- A solution to the two-fold unsupervised problem is proposed by leveraging an intrinsic property of anomalies, *i.e.*, their scarcity.
- A UDA method for one-class anomaly detection is introduced, leveraging a Vision Language Model, namely CLIP [30], for dominant cluster identification and alignment using a contrastive strategy.
- Extensive experiments and analysis are conducted on several benchmarks [20, 28, 35, 41], demonstrating the relevance of the proposed framework under both fully unsupervised and few-shot settings.

Paper Organization. Section 2 reviews UAD works under domain shift. Section 3 defines the two-fold unsupervised curse, while Section 4 and Section 5 detail the proposed solution for solving it. Section 6 and Section 7 cover the experiments and limitations of this method. Section 8 concludes and outlines future work.

2. Related Works: Anomaly detection under domain shift

Unsupervised image anomaly detection is a well-established research area [8, 13, 16, 33, 34, 38, 40] where the aim is to learn a function ζ using a single class corresponding to normal data from the normal-only dataset $\mathcal{D}^n = \{(\mathbf{X}_i, y_i); y_i = 0\}_{i=1}^N$, to classify whether an input image \mathbf{X} is normal ($y = 0$) or not ($y = 1$). This is achieved by optimizing the following objective,

$$\min_{\zeta} \mathbb{E}_{(\mathbf{X}_i, y_i) \sim \mathcal{D}^n} [\mathcal{L}(\zeta(\mathbf{X}_i), y_i = 0)], \quad (1)$$

where \mathcal{L} is a loss enforcing feature compactness as in DSVDD [33] or a reconstruction loss typically used in

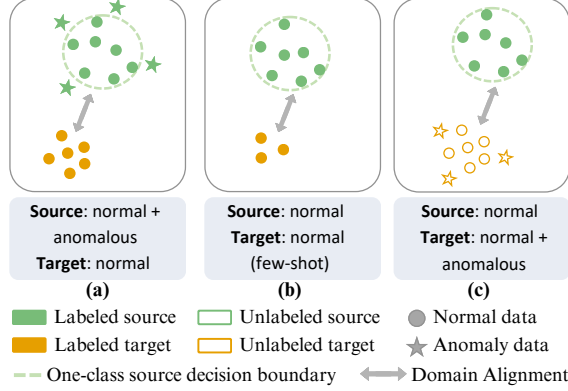


Figure 2. **Comparison of our setting with previous works:** (a) supervised source anomaly detection with supervised domain adaptation [19], (b) unsupervised one-class source anomaly detection with few-shot domain adaptation [22, 23, 43], (c) **our considered setting:** unsupervised one-class source anomaly detection with unsupervised domain adaptation.

autoencoders-based methods [8, 40]. Although achieving impressive performance on standard benchmarks, the majority of AD methods [8, 13, 16, 33, 34, 38, 40] overlook the domain gap problem where training and testing data denoted as \mathcal{D}^s and \mathcal{D}^t , respectively, follow different distributions due to uncontrolled variations in the acquisition setting [4, 5]. This domain shift induces, therefore, a significant drop in performance. To solve this issue, a handful of Domain Generalization (DG) methods for UAD has been proposed recently [4–6]. Cohen et al. [6] propose a domain-disentanglement approach that removes predefined nuisance attributes (e.g., pose, lighting) from the source features using contrastive loss, preventing these factors from interfering with the anomaly task, improving the performance on unseen domains. However, without an actual target set, this method requires defining and labeling nuisance factors within the source dataset, which is challenging, as mentioned in their paper. In [5], multiple source domains are considered for learning domain-invariant features, thereby assuming the availability of diverse large-scale datasets, which is not always guaranteed. To avoid relying on multiple domains during training, a self-supervised strategy is adopted in [4]. Nevertheless, the success of this approach heavily depends on the similarity between the augmented data and target samples. As a result, it necessitates tailoring augmentation techniques to unseen target datasets, if at all possible. Given its effectiveness, domain adaptation has also been explored to address the domain shift problem in AD [7, 19, 21–23]. Those techniques usually adopt a few-shot adaptation paradigm by having access to a limited number of annotated target samples. While these methods offer innovative solutions for aligning source and target normal data, they still rely on costly annotations [16] and are exposed to overfitting risks [37]. This

emphasizes the need for a fully unsupervised domain adaptation for UAD. However, solving this challenge remains challenging given the doubly unsupervised nature of the problem resulting from both UAD and UDA, which is further described in the next section.

3. The Two-fold Unsupervised Curse

Let us denote as $\mathcal{D}^s = \{(\mathbf{X}_i^s, y_i^s)\}_{i=1}^{N_s}$ a labeled dataset from a given domain called *source* formed by N_s samples, where a sample $\mathbf{X}_i^s \in \mathbb{R}^{h \times w \times c}$ and its associated label $y_i^s \in \{0, 1\}$, $\forall i = \{1, \dots, N_s\}$. Let \mathcal{D}^t be a second unlabeled dataset from a different domain, i.e., *target*, denoted as $\mathcal{D}^t = \{\mathbf{X}_i^t\}_{i=1}^{N_t}$ and formed by N_t samples where $\mathbf{X}_i^t \in \mathbb{R}^{h \times w \times c}$, $\forall i = \{1, \dots, N_t\}$. In the following, we assume that \mathcal{D}^t shares the same label space as \mathcal{D}^s and that there exists a domain gap between \mathcal{D}^s and \mathcal{D}^t . The goal of Unsupervised Domain Adaptation (UDA) for anomaly detection (whether formulated as a binary or one-class classification problem), is to learn a model $\zeta : \mathbb{R}^{h \times w \times c} \rightarrow \{0, 1\}$ using both \mathcal{D}^s and \mathcal{D}^t that generalizes to the target domain. In other words, it aims at learning a domain invariant feature extractor $f : \mathbb{R}^{h \times w \times c} \mapsto \mathcal{X}$ such that $\zeta = g \circ f$ with $g : \mathcal{X} \mapsto \{0, 1\}$ being the classifier and \mathcal{X} the feature space given by f . This objective is achieved by minimizing the following adaptation upper bound [2],

$$\epsilon^t \leq \epsilon^s + d(f(\mathcal{D}^s), f(\mathcal{D}^t)) + \lambda, \quad (2)$$

where ϵ_t and ϵ_s are the expected classification errors on the target and source domains, respectively; $d(f(\mathcal{D}^s), f(\mathcal{D}^t))$ estimates the discrepancy between the feature distributions from the two domains, and λ accounts for the error of an ideal detector.

While strategies for minimizing this upper bound are feasible in the context of binary or even multi-class classification [18, 36, 42], the non-availability of anomalous data during training makes it difficult in the context of one-class classification, where $d(f(\mathcal{D}^s), f(\mathcal{D}^t))$ cannot be estimated. In fact, we can only use a subset $\mathcal{D}^{s,n} \subset \mathcal{D}^s$ formed by normal data for training. For that reason, existing works on domain adaptation for one-class anomaly detection [7, 22, 43] revisit the formulation given in Eq (2) by slightly simplifying the problem. They pose it as a few-shot domain adaptation setting (instead of a fully unsupervised scenario). This means that they assume having access to a small subset $\mathcal{D}^{t,n} \subset \mathcal{D}^t$ composed of normal samples only. As a result, they reformulate Eq (2) as follows,

$$\epsilon^{t,n} \leq \epsilon^{s,n} + d(f(\mathcal{D}^{s,n}), f(\mathcal{D}^{t,n})) + \lambda. \quad (3)$$

where $\epsilon^{s,n}$ and $\epsilon^{t,n}$ represent the source and target expected classification errors related to the normal class, respectively, since ϵ^s is not measurable in this context.

Nevertheless, in a fully unsupervised setting, we have access to $\mathcal{D}^t = \mathcal{D}^{t,a} \cup \mathcal{D}^{t,n}$ where $\mathcal{D}^{t,a}$ represents the subset of \mathcal{D}^t formed by anomalies, without any prior information regarding the labels. Hence, directly aligning the feature distributions estimated from the source and target data by approximating $d(f(\mathcal{D}^{s,n}), f(\mathcal{D}^t))$ would lead to obtaining a classification boundary that is completely obsolete for target data, as shown in Figure 1 (b). We call this problem the *two-fold unsupervised curse* as it is a consequence of a lack of supervision: (1) in the task of anomaly detection, as it is formulated as a one-class problem where only normal source data are used; and (2) in the task of domain adaptation which is fully unsupervised where only an unlabeled target set is available. Given that the problem is ill-posed, it remains a significant challenge that has not been addressed in the existing UAD literature.

4. Rare Anomalies to the Rescue

To tackle the two-fold unsupervised curse described in Section 3, we introduce a key assumption and the main hypothesis it entails for enabling unsupervised domain adaptation for one-class anomaly detection.

Assumption (anomaly scarcity). *For an unlabeled target dataset $\mathcal{D}^t = \mathcal{D}^{t,n} \cup \mathcal{D}^{t,a}$, we assume that the number of anomalous samples is significantly smaller than the number of normal samples, i.e., $|\mathcal{D}^a| \ll |\mathcal{D}^n|$, with $|\cdot|$ refers to the cardinality.*

Hypothesis (dominant cluster existence). *Considering a target unlabeled anomaly detection dataset $\mathcal{D}^t = \mathcal{D}^{t,n} \cup \mathcal{D}^{t,a}$ under the anomaly scarcity assumption, where $\mathcal{D}^{t,n}$ and $\mathcal{D}^{t,a}$ are respectively the normal and abnormal subsets, we hypothesize that there exists a feature extractor $\psi: \mathbb{R}^{h \times w \times c} \rightarrow \mathcal{X}$ that generates from \mathcal{D}^t a compact dominant cluster $\mathcal{C} \in \mathcal{X}$ predominated by normal samples.*

The anomaly scarcity assumption often holds as it reflects most real-world scenarios where anomalies are rare compared to normal instances. In summary, our main objective is, therefore, to find or learn a feature extractor that verifies the dominant cluster existence hypothesis. This hypothesis is a core component of the proposed method discussed in Section 5, as it allows the introduction of a novel paradigm to approach UDA for one-class UAD consisting of (1) finding a feature extractor ψ that can generate a compact dominant cluster of features \mathcal{C} corresponding to normal samples within an unlabeled target dataset \mathcal{D}^t , (2) identifying the subset of samples $\tilde{\mathcal{D}}^{t,n}$ corresponding to this cluster in the feature space of ψ , and (3) aligning the identified subset $\tilde{\mathcal{D}}^{t,n}$ with the source normal samples $\mathcal{D}^{s,n}$ in the feature space of the source feature extractor f . Formally, we revisit Eq (3) as follows,

$$\epsilon^{t,n} \leq \epsilon^{s,n} + d(f(\mathcal{D}^{s,n}), f(\tilde{\mathcal{D}}^{t,n})) + \lambda, \quad (4)$$

where $\tilde{\mathcal{D}}^{t,n} = \{\mathbf{X}_i^t \mid \psi(\mathbf{X}_i^t) \in \mathcal{C}\}$. Note that ψ can be obtained by focusing on learning compact cross-domain features from which \mathcal{C} can be identified through feature grouping and selection techniques such as clustering or filtering. As such, the proposed paradigm for UDA in one-class UAD lays the foundation for future research, where various technical choices can be explored at each stage.

5. Proposed Solution to the Two-fold Unsupervised Curse

Building on the assumption and hypothesis formulated in Section 4, we present the technical choices, implemented as one possible solution for addressing UDA for semantic one-class-based image UAD, as illustrated in Figure 3.

Our approach has two branches. The upper branch depicts a trainable backbone f that learns from both source and target domain data. The source features are optimized using a Deep Support Vector Data Description (DSVDD) objective [33]. The lower branch focuses on visual feature extraction from the unlabeled target domain, through a frozen CLIP visual encoder [30], defined as the ψ feature extractor. Clustering is applied to these visual features to estimate the dominant cluster \mathcal{C} . Samples identified within \mathcal{C} in the ψ visual encoder’s representation space are then selected within the space of the feature extractor f and then aligned with the normal source features. An algorithm is provided in Section A of the Supplementary.

Training. Specifically, given source and target image datasets $\mathcal{D}^{s,n}$ and \mathcal{D}^t , we apply DSVDD on the source data, enforcing feature compactness by minimizing the radius of a hypersphere to encapsulate the normal source representations. This is done by solving the following optimization problem,

$$\min_{\theta_f} \mathcal{L}_{AD} = \min_{\theta_f} \frac{1}{N_s} \sum_{i=1}^{N_s} \|f(\mathbf{X}_i^s) - \boldsymbol{\mu}^{s,n}\|_2^2, \forall \mathbf{X}_i^s \in \mathcal{D}^{s,n}, \quad (5)$$

where $\boldsymbol{\mu}^{s,n}$ is the mean of the source features. For clustering, we use a K -means algorithm. Note that ψ can be f itself or any frozen visual encoder such as CLIP [30] or DINO-v2 [27]. The dominant cluster is identified as,

$$\mathcal{C} = \arg \max_{\mathcal{C}_k} |\mathcal{C}_k| \text{ for } k \in \{1, \dots, K\}, \quad (6)$$

where $|\mathcal{C}_k|$ is the size of the k -th cluster \mathcal{C}_k , and K is a hyper-parameter defining the number of expected components in the space of $\psi(\mathcal{D}^t)$. When clustering is applied to $f(\mathcal{D}^t)$, the selected features for alignment are $\tilde{\mathcal{D}}^{t,n} = \mathcal{C}$. When clustering is applied to $\psi(\mathcal{D}^t)$, the selected samples are:

$$\tilde{\mathcal{D}}^{t,n} = \{f(\mathbf{X}_i^t) \mid \psi(\mathbf{X}_i^t) \in \mathcal{C}\} \forall \mathbf{X}_i^t \in \mathcal{D}^t \quad (7)$$

Alignment between source and target features is achieved using a contrastive strategy, where the loss of a single positive source-target pair $\ell_{i,j}$:

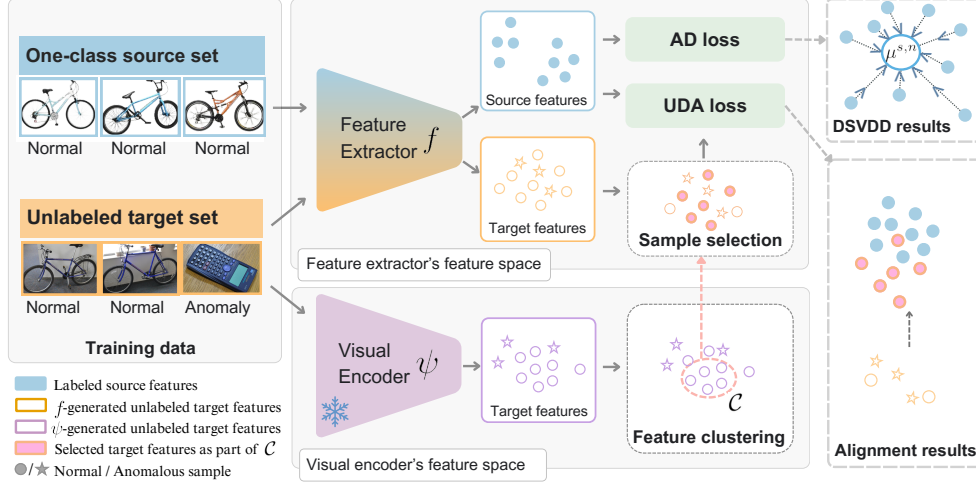


Figure 3. **Overview of the proposed method:** The top branch uses a trainable feature extractor with a DSVDD objective for one-class source data. The bottom branch clusters the features using a frozen CLIP visual encoder to identify the dominant feature cluster and align it with normal source representations. ● and ★ denote normal and anomalous samples respectively.

$$\ell_{i,j} = -\log \frac{\exp\left(\frac{1}{\tau} \cdot \text{sim}(f(\mathbf{X}_i^s), f(\mathbf{X}_j^t))\right)}{\sum_{p=1}^{N_t} \mathbb{1}_{[\mathbf{X}_p^t \notin \tilde{\mathcal{D}}^{t,n}]} \exp\left(\frac{1}{\tau} \cdot \text{sim}(f(\mathbf{X}_i^s), f(\mathbf{X}_p^t))\right)} \quad (8)$$

where $\text{sim}(\cdot, \cdot)$ denotes the cosine similarity, and τ is a temperature hyper-parameter. The UDA loss is computed as:

$$\mathcal{L}_{UDA} = \frac{1}{N_s \times |\tilde{\mathcal{D}}^{t,n}|} \sum_{i=1}^{N_s} \sum_{j=1}^{|\tilde{\mathcal{D}}^{t,n}|} \ell_{i,j}, \quad (9)$$

Finally, the overall loss is given by:

$$\mathcal{L} = \lambda_1 \mathcal{L}_{AD} + \lambda_2 \mathcal{L}_{UDA}, \quad (10)$$

where λ_1 and λ_2 are hyper-parameters for \mathcal{L}_{AD} and \mathcal{L}_{UDA} .

Inference. Note that the visual encoder ψ is discarded at inference and that only the feature extractor f is used to determine whether the input data is anomalous by calculating whether it falls inside or outside the hypersphere estimated by the DSVDD model. Our method’s algorithm is given in Section A of the Supplementary.

6. Experimental Results

6.1. Experimental Setting

This section describes the datasets and the baselines used and the implementation details of our experiments. We report the performance using Area Under the ROC Curve (AUC) using **bold** and underline for the best and second performances, respectively. The supplementary materials provide further details on each subsection.

Datasets. We evaluate our approach on four standard UDA benchmark datasets, **Office-Home** [35], **Office31** [35], **VisDA** [28], and **PACS** [20]. The types of domain shift of each dataset is described in Section A of the

Supplementary. For the AD task, we adopt a standard one-vs-all protocol, where a single class is considered normal and the remaining are anomalies. We adopt the experimental protocol of previous DA works [7, 22, 43] to allow for a fair comparison –that is, we show results on ten classes from the ClipArt and Product domains for Office-Home, ten classes from Webcam and Amazon for Office31, and twelve classes from the domains of Computer Aided Designs (CAD) (synthetic objects) and real object photos of VisDA. On PACS, like [4], we consider the Photo domain as source and the remaining three domains as targets.

Baselines. As no other works on UDA for semantic image UAD were previously introduced, we compare our method with several few-shot SoA approaches. More specifically, we consider **BiOST** [7] which is a one-shot approach and **TSA** [21], **ILDR** [19], **IRAD** [43], and **MsRA** [22] that are few-shot methods. Furthermore, we introduce a few-shot variant (**Ours-Few-shot**) of our approach, which augments the target domain with normal and pseudo-anomalous samples similar to [11]. This augmentation yields semantically positive and negative pairs [11], which are useful for the contrastive alignment strategy described in Section 5. Further details are given in Section A of the Supplementary.

Implementation details. In all experiments, the source set has only normal data, while the unlabeled target set includes mostly normals with 10% randomly sampled anomalies. Training uses SGD with a cosine-annealing scheduler, learning rate of 10^{-3} , weight decay of 5×10^{-7} , batch size 256 and λ_1 and λ_2 are set to 1. CLIP-ViT-B32 is the frozen visual encoder ψ for feature clustering. To align with the setting of the baselines [7, 21, 22, 43], ResNet50 is the trainable backbone f , initialized on ImageNet [9]. K-

Normal class	Source only DSVDD	Few-shot						Unsupervised	Normal class	Source only DSVDD	Few-shot						Unsupervised	
		BiOST	TSA	ILDR	IRAD	MsRA	Ours				Ours	BiOST	TSA	ILDR	IRAD	MsRA		Ours
Clip Art \rightarrow Product (C \rightarrow P)									Webcam \rightarrow Amazon (W \rightarrow A)									
Bike	97.48	43.00	69.10	89.90	90.30	94.30	98.34	85.71	Backpack	86.48	59.90	76.30	91.90	90.20	95.20	95.40	97.62	
Calculator	83.47	69.00	72.20	84.90	82.20	98.70	97.76	97.70	Bookcase	35.77	56.60	59.60	78.40	82.20	84.50	76.25	91.16	
Drill	81.57	66.40	66.20	75.30	73.00	84.50	74.19	96.64	Bottle	70.00	60.80	66.80	74.50	72.10	74.00	72.48	77.32	
Hammer	83.32	50.10	77.40	74.70	84.50	80.10	89.55	82.63	Desk Chair	56.92	57.60	63.40	85.30	80.90	87.20	85.50	92.06	
Kettle	87.74	63.00	63.10	77.50	75.80	85.50	94.08	89.16	Desk Lamp	82.26	50.50	60.90	72.60	67.50	70.00	82.38	81.50	
Knives	78.09	48.80	51.90	55.20	63.90	64.40	79.25	76.63	Headphones	88.91	57.60	75.90	88.90	81.60	92.20	92.53	95.06	
Pan	74.00	57.70	63.70	72.20	76.00	80.50	93.08	91.07	Keyboard	79.83	58.20	69.90	88.30	93.20	95.40	95.40	93.36	
Paperclip	53.04	27.40	74.70	78.70	67.40	79.70	71.18	67.98	Laptop	51.79	59.10	63.00	86.20	98.10	99.00	95.63	79.97	
Scissors	86.45	56.40	64.70	79.50	68.90	85.50	87.71	88.43	Mouse	83.95	65.80	53.40	84.90	79.60	89.90	96.65	92.97	
Soda	51.21	50.20	57.40	70.30	53.30	72.40	61.16	92.37	Pen	48.54	68.50	69.10	75.50	71.40	73.90	72.72	71.20	
Avg.	77.64	53.20	66.04	75.82	73.53	82.56	84.63	86.83	Avg.	68.45	59.46	65.83	82.65	81.68	86.13	86.49	87.22	
\pm std	± 14.04	± 11.65	± 7.36	± 8.81	± 10.24	± 9.33	± 11.93	± 8.66	\pm std	± 17.84	± 4.70	± 6.86	± 6.46	± 9.37	± 9.72	± 9.44	± 8.48	
Product \rightarrow Clip Art (P \rightarrow C)									Amazon \rightarrow Webcam (A \rightarrow W)									
Bike	82.55	52.70	65.80	83.10	85.70	86.60	82.06	92.99	Backpack	79.42	47.90	59.00	81.60	91.20	97.50	99.28	97.59	
Calculator	62.82	65.20	63.40	87.20	79.20	91.90	91.59	89.88	Bookcase	60.68	49.90	72.30	88.90	89.40	93.10	85.23	94.29	
Drill	71.81	47.00	57.10	63.90	71.20	73.50	70.58	77.54	Bottle	40.94	66.00	69.80	86.90	95.30	96.20	93.65	94.95	
Hammer	68.02	43.70	68.60	60.20	77.00	73.00	84.33	65.42	Desk Chair	71.66	67.00	66.20	76.10	90.30	90.10	93.67	99.08	
Kettle	71.85	47.70	61.50	68.80	70.00	73.40	75.38	78.19	Desk Lamp	94.63	55.50	68.60	73.10	81.30	83.90	94.57	97.61	
Knives	57.22	63.10	57.50	65.30	70.30	73.10	77.74	71.99	Headphones	70.99	68.30	72.40	93.70	91.60	96.00	96.54	96.04	
Pan	71.44	49.30	63.50	69.30	72.80	80.00	83.72	82.46	Keyboard	77.90	66.00	76.90	91.10	95.70	98.10	90.62	76.59	
Paperclip	26.19	45.10	49.90	69.70	61.80	69.00	67.05	55.93	Laptop	91.61	62.10	72.20	85.70	97.10	98.20	94.32	97.67	
Scissors	63.42	38.60	70.10	66.20	70.00	72.30	86.35	77.63	Mouse	72.17	69.10	69.40	82.20	85.40	86.50	96.35	81.41	
Soda	66.82	56.90	55.80	60.20	63.29	59.40	69.08	62.63	Pen	44.26	79.10	86.10	97.60	98.90	99.60	97.09	99.99	
Avg.	64.21	50.93	61.32	69.39	72.13	75.22	78.79	75.47	Avg.	70.43	63.09	71.29	85.69	91.62	93.92	94.13	93.52	
\pm std	± 14.22	± 8.11	± 5.94	± 8.55	± 6.76	± 8.62	± 7.74	± 11.13	\pm std	± 16.81	± 9.03	± 6.66	± 7.26	± 5.15	± 5.11	± 3.72	± 7.52	
(a) OfficeHome [41]									(b) Office31 [35]									

(a) OfficeHome [41]

(b) Office31 [35]

Table 1. Ten-run average and standard deviation of AUC (%) on the Office datasets against previous SoA.

Normal class	Source only (DSVDD)	Few-shot			Unsup.
		BiOST	MsRA	Ours	Ours
Synthetic (CAD) \rightarrow Real					
Aero.	67.71	36.80	81.56	81.55	84.86
Bicycle	65.12	59.20	68.45	74.58	81.45
Bus	66.01	47.90	68.12	72.26	82.17
Car	78.65	53.80	69.44	82.78	62.76
Horse	67.24	58.00	68.77	80.17	83.52
Knife	62.43	54.10	70.39	71.52	68.82
Motor.	69.45	58.10	65.64	80.16	91.15
Person	42.11	58.70	59.18	51.24	69.68
Plant	57.77	42.10	65.81	71.46	70.58
Skate.	60.70	41.60	61.30	63.17	83.71
Train	54.75	52.40	69.73	60.62	69.98
Truck	62.08	43.10	59.05	73.67	57.84
Avg.	62.84	50.48	67.28	71.93	75.54
\pm std	± 8.55	± 7.55	± 5.79	± 9.08	± 9.80

Table 2. Ten-run average and standard deviation of AUC (%) on the on the VisDA dataset [28] against previous SoA.

means clustering [14] uses 2, 10, and 5 components for Office, VisDA, and PACS, respectively. Like the baselines, the few-shot experiments use 10 (Office, PACS) and 100 shots (VisDA) labeled as normal, respectively.

6.2. Comparison against State-of-the-art.

Our method outperforms previous SoA on all benchmarks of our evaluation, as shown in Table 1 and Table 2. More specifically, our fully unsupervised UDA-UAD importantly improves upon previous few-shot SoA on $C \rightarrow P$ and $W \rightarrow A$ of the Office-Home [41] and Office31 [35] datasets.

In addition, we observe an improvement of over 10% in the VisDA dataset [28] with the fully unsupervised methodology over previous few-shot approaches despite being challenged by the two-fold unsupervised curse. These results highlight the relevance of the proposed method, even in the presence of a large domain gap, as in the case of synthetic CAD images and real-world photos.

In the $P \rightarrow C$ and $A \rightarrow W$ adaptation of the Office datasets, our few-shot variant also registers SoA performance, closely followed by our model trained under the fully unsupervised setting. These results highlight the flexibility of our framework, which can leverage minimal labeled target data when available but remains highly effective in a fully unsupervised setting.

Furthermore, we compare the performance of our model to two pretrained visual encoders [30], namely ResNet50 and CLIP-ViT-B32 in Table 3. While the CLIP-ViT-B32 architecture achieves an average AUC of 72.08%, our unsupervised method (75.54%) still outperforms it on the VisDA dataset [28]. In contrast, the ResNet50 shows a significantly lower performance, with an average AUC of only 53.45%. These results demonstrate that despite their strong performance, pretrained visual encoders are not specifically tailored for the domain adaptation task; thus, they remain vulnerable to domain shift. Therefore, training domain adaptation-specific models is still necessary to effectively bridge the gap between two given domains.

6.3. Additional Experiments

Unless stated otherwise, all the following experiments are performed on VisDA [28]. Additional results on different components of our method are given in the Supplementary.

Anomaly scarcity assumption. To evaluate the impact of anomaly scarcity, we vary the anomaly ratio in the unlabeled target set from 10% to 90% and report our method’s performance alongside clustering accuracy in Figure 4 for the Aeroplane class from VisDA. The results indicate a strong correlation between AUC performance and clustering accuracy. As the anomaly proportion increases, the AUC gradually degrades, with a drastic drop beyond 50%, where the dominant cluster assumption no longer holds. This is further evidenced by a significant decrease in the clustering accuracy.

Few-shot versus unsupervised paradigms.

The results presented in Table 3 compare pre-trained visual encoders and source-only detectors with different adaptation paradigms, i.e., few-shot, unsupervised, and supervised (oracle). The source-only fine-tuned model improves slightly over the pretrained ResNet50 visual encoder [15] but still has lower performance than the adaptation approaches, achieving an average AUC of 62.84%. Among the few-shot methods, our few-shot variant outperforms BiOST [7] and MsRA [22], achieving the highest AUC of 71.93%, which is comparable to the performance of a pretrained CLIP-ViT-B32 visual encoder. However, our unsupervised adaptation method surpasses all these models, with an average AUC of 75.54% indicating its ability to effectively mitigate domain gaps without relying on labeled target data. This can be explained by the fact that after clustering, our model has access to more representative normal target data than few-shot models, hence better generalizing to the target normal class. On the other hand, the Oracle, which has access to the target labels, achieves the highest performance (81.65%). The small gap between our unsupervised method and the oracle demonstrates the effectiveness of our approach even without supervision.

Ablation on the framework components. Table 4 provides the results obtained when each component, namely the adaptation loss, the dominant cluster identification through clustering, the use of an auxiliary visual encoder $\psi(\mathcal{D}^t)$ or the trainable features $f(\mathcal{D}^t)$. The results show that without adaptation, a model trained only on source data generalizes poorly to the target domain with only 62.84%. Direct adaptation of the source and the unlabeled target

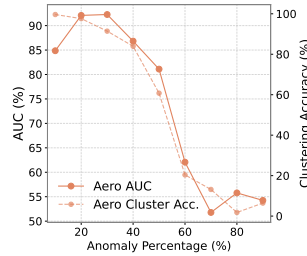


Figure 4. Assessing the validity of anomaly scarcity assumption.

Normal class	Zero-shot		DSVDD src fine- tuned only	Few-shot Adaptation			Unsup. Adapt. Ours	Super- (Adap. vised)
	R50	CLIP		BiOST	MsRA	Ours		
CAD → Real								
Aero.	41.05	74.97	67.71	36.80	81.56	81.55	84.86	90.91
Bicycle	67.35	90.28	65.12	59.20	68.45	74.58	81.45	81.73
Bus	28.58	42.27	66.01	47.90	68.12	72.26	82.17	72.16
Car	32.48	64.16	78.65	53.80	69.44	82.78	62.76	68.42
Horse	68.81	75.48	67.24	58.00	68.77	80.17	83.52	88.70
Knife	67.78	95.28	62.43	54.10	70.39	71.52	68.82	78.90
Motor.	60.07	82.25	69.45	58.10	65.64	80.16	91.15	83.46
Person	71.69	56.26	42.11	58.70	59.18	51.24	69.68	85.19
Plant	62.47	89.65	57.77	42.10	65.81	71.46	70.58	82.63
Skate.	85.00	91.52	60.70	41.60	61.30	63.17	83.71	83.73
Train	30.13	57.74	54.75	52.40	69.73	60.62	69.98	85.11
Truck	26.05	45.08	62.08	43.10	59.05	73.67	57.84	78.91
Avg.	53.45	72.08	62.84	50.48	67.28	71.93	<u>75.54</u>	81.65
±std	±19.57	±17.83	±8.55	±7.55	±5.79	±9.08	±9.80	±6.11

Table 3. AUC (%) performance on the target domain of our UDA anomaly detector on VisDA [28] compared with various adaptation paradigms (from zero-shot, i.e., pretrained Visual encoders, few-shot, to supervised, i.e., Oracle).

w/ Adaptation	w/ Clustering	w/ CLIP ψ	AUC (%)
✗	✗	✗	62.84±8.55
✓	✗	✗	64.33±6.42
✓	✓	✗	68.47±8.30
✓	✓	✓	75.54±9.80

Table 4. Ablation on the components of the proposed method.

without clustering leads to inconsistent results, indicating low generalization capabilities to the target domain. Introducing clustering results in a significant performance boost. This can be seen when clustering is applied to the original representations of the feature extractor, as the performance improves by +5.63%, highlighting the importance of identifying the dominant cluster prior to alignment. Note that our method still outperforms the best few-shot baseline MsRA [22] (68.47% vs 67.28%) with just clustering and alignment (*i.e.* w/o CLIP) across all the VisDA classes. Finally, the best results are achieved when all components are combined. This setup boosts the average AUC to 75.54% on all VisDA classes. The substantial performance gains can be attributed to CLIP’s rich visual features, which, together with clustering and alignment, help achieve a more robust anomaly detector capable of better handling domain shift.

Dataset	w/o Adapt. (Src Only)	w/ Adaptation			
		Kmeans	GMM	Meanshift	kNN
VisDA	62.84±8.55	75.54±10.23	72.24±08.81	74.14±07.44	71.65±06.68
A→W	72.57±18.69	94.82±07.52	96.45±05.43	87.32±12.53	82.73±10.96
W→A	67.70±18.32	87.72±12.63	87.00±13.60	86.68±08.53	83.63±06.04
C→P	77.31±15.13	90.54±14.06	90.85±11.18	85.95±10.94	78.67±15.19
P→C	63.88±15.60	70.92±11.36	76.15±13.32	73.50±13.49	71.38±11.71

Table 5. Ablation on different clustering techniques. GMM and K-means use 10 components for VisDA and 2 for other datasets. k=2 for VisDA and k=1 for the remaining datasets.

Clustering methods. We compare different clustering techniques on three UDA benchmarks in Table 5. The first observation we make is that any type of clustering improves the performance. K-means and GMM have comparable results, without one clearly and consistently outperforming the other across datasets and adaptation directions. Mean-shift clustering offers a performance increase compared to source-only models. However, its performance remains lower than that of the other clustering methods. In our experiments, we chose K-means clustering as it achieves comparable performance to GMM while requiring fewer parameters and simpler optimization. We further investigate the optimal number of K-Means components, as shown in Figure 5. The figure indicates that using 8 to 10 components yields the highest performance, with an AUC of approximately 75-76%. Decreasing the number of components would gradually degrade the performance. This suggests that a lower number of clusters may not capture the characteristics of the majority class, leading to inaccurate clustering and thus negatively impacting the generalization of the anomaly detection model across domains.

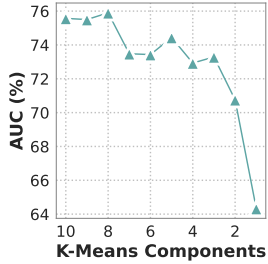


Figure 5. K-Means[14] components variation on VisDA.

<i>f</i> : ResNet50 + <i>ψ</i> : CLIP-ViT-B32					
DSVDD [33]			MSC [31]		
ZS	Src	UDA	ZS	Src	UDA
53.45	62.84	75.54	74.39	72.87	81.10
		(+12.7↑)			(+8.23↑)

Table 6. Our UDA approach on two anomaly detection methods: DSVDD [33] and Mean-shifted Contrastive Learning (MSC) [31]. ZS and Src mean Zero-shot and Source only, respectively.

Beyond DSVDD. To assess whether our alignment approach applies to other unsupervised AD methods, we replace DSVDD with Mean-shifted Contrastive loss (MSC) [31] in Table 6. MSC adapts contrastive loss to the one-class setting by shifting augmented representations of the normal samples toward the mean of pretrained normal features, preserving their compactness. Similar to [6, 32], it uses a kNN density estimator to detect anomalies. Our results suggest that both methods benefit from the adaptation, as a consistent average improvement of +12.7% and +8.23% is seen across all the 12 classes of VisDA.

Alignment strategies. By comparing several alignment strategies in Table 7, we observe that any alignment strategy, in general, improves the performance consistently for all adaptation benchmarks. Contrastive alignment consistently outperforms other adaptation losses, including statistical (MMD) [12] and adversarial (GRL) [10] strategies.

Dataset	Source Only	GRL [10]	MMD [12]	Contrastive [26]
VisDA	62.84±08.55	71.84±10.89	73.12±10.36	75.54±9.80
A→W	72.57±18.69	90.43±10.68	86.86±12.97	94.82±07.52
W→A	67.70±18.32	83.49±11.04	83.92±09.90	87.72±12.63
C→P	77.31±15.13	83.40±12.35	82.10±12.16	90.54±14.06
P→C	63.88±15.60	66.78±15.02	67.00±14.41	70.92±11.35

Table 7. Performance in terms of AUC (%) using different adaptation losses on the three UDA benchmarks.

Comparison against domain generalization methods. Table 8 compares the results of GNL [4] with our proposed UDA method on the PACS dataset [20], with Photo as the source and Art, Cartoon, and Sketch as the target domains. It can be seen that our UDA approach consistently outperforms GNL [4], particularly on Cartoon and Sketch domains. This suggests that unlike DG methods, which aim to generalize to any unseen domain solely by training on the source domain, UDA can be more effective for semantic UAD since it exposes the model to the target domain during training, even if it is unlabeled.

Adapt. Type	Method	Ph. → Art	Ph. → Cartoon	Ph. → Sketch
None	Source only	64.06	64.08	57.35
DG	GNL [4]	65.62	67.96	<u>62.39</u>
DA	MsRA [22] (Few-shot)	71.43	<u>69.89</u>	61.87
	Ours (Unsup.)	<u>67.20</u>	75.35	74.04

Table 8. AUC (%) of Domain Generalization (DG) for anomaly detection, trained **ONLY** on the source domain Photo (Ph.) and tested on unseen domains. DA means Domain Adaptation.

7. Limitations and Future Work

Our method, presented in Section 5, is one possible solution for addressing the problem of UDA for UAD. However, it is worth noting that it was tested in the context of semantic anomaly detection [38], adopting a one-vs-all protocol, to facilitate the comparison with the closest baselines, namely [22, 43]. These methods typically require the use of global features in contrast to standard anomaly detection, where fine-grained representations are usually targeted. For that reason, our method focuses mostly on global representations, while local features would be conceptually more suitable for fine-grained anomaly detection. In future works, we aim to extend our study to fine-grained anomaly detection by exploiting more relevant local representations.

8. Conclusion

This work is the first to address unsupervised domain adaptation (UDA) for one-class-based unsupervised anomaly detection (UAD), subject to what we refer to as the two-fold unsupervised curse. To address this ill-posed problem, an inherent property of anomalies, namely, their scarcity, is leveraged. This characteristic allows utilizing clustering, –as one possible solution– for identifying a

dominant cluster within the unlabeled target set. Assuming this cluster to be predominantly composed of normal data, a contrastive alignment strategy is then used to align its features with the normal source representations. Extensive experiments on standard UDA benchmarks demonstrate that the proposed method effectively mitigates the domain gap and enhances anomaly detection performance across different domains, outperforming other supervised adaptation approaches without requiring target annotations. Finding the optimal feature extractor remains an open research question. In future work, we intend to further explore compact representations across domains to improve the proposed domain adaptation framework.

References

- [1] Jinan Bao, Hanshi Sun, Hanqiu Deng, Yinsheng He, Zhaoxiang Zhang, and Xingyu Li. Bmad: Benchmarks for medical anomaly detection. In *Proceedings of the IEEE/CVF Conference on Computer Vision and Pattern Recognition (CVPR) Workshops*, pages 4042–4053, 2024. 1, 2
- [2] Shai Ben-David, John Blitzer, Koby Crammer, and Fernando Pereira. Analysis of representations for domain adaptation. In *Advances in Neural Information Processing Systems*. MIT Press, 2006. 3
- [3] Marius Beul, David Droeschel, Matthias Nieuwenhuisen, Jan Quenzel, Sebastian Houben, and Sven Behnke. Fast autonomous flight in warehouses for inventory applications. *IEEE Robotics and Automation Letters*, 3(4):3121–3128, 2018. 1
- [4] Tri Cao, Jiawen Zhu, and Guansong Pang. Anomaly detection under distribution shift. In *Proceedings of the IEEE/CVF International Conference on Computer Vision*, pages 6511–6523, 2023. 1, 3, 5, 8
- [5] João Carvalho, Mengtao Zhang, Robin Geyer, Carlos Cotrini, and Joachim M Buhmann. Invariant anomaly detection under distribution shifts: a causal perspective. *Advances in Neural Information Processing Systems*, 36, 2024. 3
- [6] Niv Cohen, Jonathan Kahana, and Yedid Hoshen. Red panda: Disambiguating image anomaly detection by removing nuisance factors. In *The Eleventh International Conference on Learning Representations*, 2023. 3, 8
- [7] Tomer Cohen and Lior Wolf. Bidirectional one-shot unsupervised domain mapping. In *Proceedings of the IEEE/CVF international conference on computer vision*, pages 1784–1792, 2019. 2, 3, 5, 7
- [8] Hanqiu Deng and Xingyu Li. Anomaly detection via reverse distillation from one-class embedding. In *Proceedings of the IEEE/CVF conference on computer vision and pattern recognition*, pages 9737–9746, 2022. 1, 2, 3
- [9] Jia Deng, Wei Dong, Richard Socher, Li-Jia Li, Kai Li, and Li Fei-Fei. Imagenet: A large-scale hierarchical image database. In *2009 IEEE conference on computer vision and pattern recognition*, pages 248–255. Ieee, 2009. 5
- [10] Yaroslav Ganin and Victor Lempitsky. Unsupervised domain adaptation by backpropagation. In *International conference on machine learning*, pages 1180–1189. PMLR, 2015. 8
- [11] Songwei Ge, Shlok Mishra, Chun-Liang Li, Haohan Wang, and David Jacobs. Robust contrastive learning using negative samples with diminished semantics. *Advances in Neural Information Processing Systems*, 34:27356–27368, 2021. 5
- [12] Arthur Gretton, Karsten Borgwardt, Malte Rasch, Bernhard Schölkopf, and Alex Smola. A kernel method for the two-sample-problem. *Advances in neural information processing systems*, 19, 2006. 8
- [13] Songqiao Han, Xiyang Hu, Hailiang Huang, Minqi Jiang, and Yue Zhao. Adbench: Anomaly detection benchmark. *Advances in Neural Information Processing Systems*, 35: 32142–32159, 2022. 1, 2, 3
- [14] John A Hartigan and Manchek A Wong. Algorithm as 136: A k-means clustering algorithm. *Journal of the royal statistical society. series c (applied statistics)*, 28(1):100–108, 1979. 6, 8
- [15] Kaiming He, Xiangyu Zhang, Shaoqing Ren, and Jian Sun. Deep residual learning for image recognition. In *Proceedings of the IEEE conference on computer vision and pattern recognition*, pages 770–778, 2016. 2, 7
- [16] Romain Hermaty, Vincent Gaudilliere, Abd El Rahman Shabayek, and Djamila Aouada. Removing geometric bias in one-class anomaly detection with adaptive feature perturbation. In *IEEE Winter Conference on Applications of Computer Vision, WACV 2025, Tucson, AZ, USA, February 28–March 4, 2025*. IEEE, 2025. 1, 2, 3
- [17] Chaoqin Huang, Aofan Jiang, Jinghao Feng, Ya Zhang, Xinchao Wang, and Yanfeng Wang. Adapting visual-language models for generalizable anomaly detection in medical images. In *Proceedings of the IEEE/CVF Conference on Computer Vision and Pattern Recognition*, pages 11375–11385, 2024. 1, 2
- [18] Tarun Kalluri, Sreyas Ravichandran, and Manmohan Chandraker. Uda-bench: Revisiting common assumptions in unsupervised domain adaptation using a standardized framework. *ECCV*, 2024. 2, 3
- [19] Atsutoshi Kumagai, Tomoharu Iwata, and Yasuhiro Fujiwara. Transfer anomaly detection by inferring latent domain representations. In *Advances in Neural Information Processing Systems*. Curran Associates, Inc., 2019. 2, 3, 5
- [20] Da Li, Yongxin Yang, Yi-Zhe Song, and Timothy M Hospedales. Deeper, broader and artier domain generalization. In *Proceedings of the IEEE international conference on computer vision*, pages 5542–5550, 2017. 2, 5, 8
- [21] Shuang Li, Mixue Xie, Kaixiong Gong, Chi Harold Liu, Yulin Wang, and Wei Li. Transferable semantic augmentation for domain adaptation. In *Proceedings of the IEEE/CVF conference on computer vision and pattern recognition*, pages 11516–11525, 2021. 3, 5
- [22] Shuang Li, Shugang Li, Mixue Xie, Kaixiong Gong, Jianxin Zhao, Chi Harold Liu, and Guoren Wang. End-to-end transferable anomaly detection via multi-spectral cross-domain representation alignment. *IEEE Transactions on Knowledge and Data Engineering*, 35(12):12194–12207, 2023. 2, 3, 5, 7, 8
- [23] Yachun Li, Ying Lian, Jingjing Wang, Yuhui Chen, Chun-mao Wang, and Shiliang Pu. Few-shot one-class domain

- adaptation based on frequency for iris presentation attack detection. In *ICASSP 2022-2022 IEEE International Conference on Acoustics, Speech and Signal Processing (ICASSP)*, pages 2480–2484. IEEE, 2022. 2, 3
- [24] Jiaqi Liu, Guoyang Xie, Jinbao Wang, Shangnian Li, Chengjie Wang, Feng Zheng, and Yaochu Jin. Deep industrial image anomaly detection: A survey. *Machine Intelligence Research*, 21(1):104–135, 2024. 1, 2
- [25] Nesryne Mejri, Laura Lopez-Fuentes, Kankana Roy, Pavel Chernakov, Enjie Ghorbel, and Djamila Aouada. Unsupervised anomaly detection in time-series: An extensive evaluation and analysis of state-of-the-art methods. *Expert Systems with Applications*, page 124922, 2024. 1
- [26] Aaron van den Oord, Yazhe Li, and Oriol Vinyals. Representation learning with contrastive predictive coding. *arXiv preprint arXiv:1807.03748*, 2018. 2, 8
- [27] Maxime Oquab, Timothée Darcet, Theo Moutakanni, Huy V. Vo, Marc Szafraniec, Vasil Khalidov, Pierre Fernandez, Daniel Haziza, Francisco Massa, Alaaeldin El-Nouby, Russell Howes, Po-Yao Huang, Hu Xu, Vasu Sharma, Shangwen Li, Wojciech Galuba, Mike Rabbat, Mido Assran, Nicolas Ballas, Gabriel Synnaeve, Ishan Misra, Herve Jegou, Julien Mairal, Patrick Labatut, Armand Joulin, and Piotr Bojanowski. Dinov2: Learning robust visual features without supervision, 2023. 4
- [28] Xingchao Peng, Ben Usman, Neela Kaushik, Judy Hoffman, Dequan Wang, and Kate Saenko. Visda: The visual domain adaptation challenge. *arXiv preprint arXiv:1710.06924*, 2017. 2, 5, 6, 7
- [29] Joaquin Quiñero-Candela, Masashi Sugiyama, Anton Schwaighofer, and Neil D. Lawrence. *Dataset shift in machine learning*. MIT Press, London, England, 2022. 1
- [30] Alec Radford, Jong Wook Kim, Chris Hallacy, Aditya Ramesh, Gabriel Goh, Sandhini Agarwal, Girish Sastry, Amanda Askell, Pamela Mishkin, Jack Clark, et al. Learning transferable visual models from natural language supervision. In *International conference on machine learning*, pages 8748–8763. PMLR, 2021. 2, 4, 6
- [31] Tal Reiss and Yedid Hoshen. Mean-shifted contrastive loss for anomaly detection. In *Proceedings of the AAAI Conference on Artificial Intelligence*, pages 2155–2162, 2023. 8
- [32] Tal Reiss, Niv Cohen, Liron Bergman, and Yedid Hoshen. Panda: Adapting pretrained features for anomaly detection and segmentation. In *Proceedings of the IEEE/CVF Conference on Computer Vision and Pattern Recognition (CVPR)*, pages 2806–2814, 2021. 8
- [33] Lukas Ruff, Robert A. Vandermeulen, Nico Görnitz, Lucas Deecke, Shoaib A. Siddiqui, Alexander Binder, Emmanuel Müller, and Marius Kloft. Deep one-class classification. In *Proceedings of the 35th International Conference on Machine Learning*, pages 4393–4402, 2018. 1, 2, 3, 4, 8
- [34] Lukas Ruff, Jacob R. Kauffmann, Robert A. Vandermeulen, Grégoire Montavon, Wojciech Samek, Marius Kloft, Thomas G. Dietterich, and Klaus-Robert Müller. A unifying review of deep and shallow anomaly detection. *Proceedings of the IEEE*, 109(5):756–795, 2021. 1, 2, 3
- [35] Kate Saenko, Brian Kulis, Mario Fritz, and Trevor Darrell. Adapting visual category models to new domains. In *Computer Vision–ECCV 2010: 11th European Conference on Computer Vision, Heraklion, Crete, Greece, September 5–11, 2010, Proceedings, Part IV 11*, pages 213–226. Springer, 2010. 2, 5, 6
- [36] Inder Pal Singh, Enjie Ghorbel, Anis Kacem, Arunkumar Rathinam, and Djamila Aouada. Discriminator-free unsupervised domain adaptation for multi-label image classification. In *Proceedings of the IEEE/CVF Winter Conference on Applications of Computer Vision*, pages 3936–3945, 2024. 2, 3
- [37] Yisheng Song, Ting Wang, Puyu Cai, Subrota K. Mondal, and Jyoti Prakash Sahoo. A comprehensive survey of few-shot learning: Evolution, applications, challenges, and opportunities. *ACM Comput. Surv.*, 55(13s), 2023. 2, 3
- [38] Luc PJ Sträter, Mohammadreza Salehi, Efstratios Gavves, Cees GM Snoek, and Yuki M Asano. Generalad: Anomaly detection across domains by attending to distorted features. *arXiv preprint arXiv:2407.12427*, 2024. 1, 2, 3, 8
- [39] Han Sun, Kevin Ammann, Stylianos Giannoulakis, and Olga Fink. Continuous test-time domain adaptation for efficient fault detection under evolving operating conditions. *arXiv preprint arXiv:2406.06607*, 2024. 1
- [40] Tran Dinh Tien, Anh Tuan Nguyen, Nguyen Hoang Tran, Ta Duc Huy, Soan T.M. Duong, Chanh D. Tr. Nguyen, and Steven Q. H. Truong. Revisiting reverse distillation for anomaly detection. In *Proceedings of the IEEE/CVF Conference on Computer Vision and Pattern Recognition (CVPR)*, pages 24511–24520, 2023. 1, 2, 3
- [41] Hemanth Venkateswara, Jose Eusebio, Shayok Chakraborty, and Sethuraman Panchanathan. Deep hashing network for unsupervised domain adaptation. In *Proceedings of the IEEE conference on computer vision and pattern recognition*, pages 5018–5027, 2017. 2, 6
- [42] Garrett Wilson and Diane J Cook. A survey of unsupervised deep domain adaptation. *ACM Transactions on Intelligent Systems and Technology (TIST)*, 11(5):1–46, 2020. 2, 3
- [43] Ziyi Yang, Iman Soltani, and Eric Darve. Anomaly detection with domain adaptation. In *Proceedings of the IEEE/CVF Conference on Computer Vision and Pattern Recognition*, pages 2958–2967, 2023. 2, 3, 5, 8